Original Article

Synthesis Method Effect on Acellular Bioactivity of Bioglasses: Structural Analysis and Solid-State NMR

Salwa El Baakili[a] | Abdelhabib Semlali[b] | Khalil El Mabrouk[a] | Meriame Bricha[a,*]

[a]*Euromed Research Center, Euromed Polytechnic School, Euromed University of Fes, Eco-Campus, Meknes Road, 30 030 Fes, Morocco*
[b]*Ecology Research Group, Faculty of Dentistry, Laval University, Quebec City (QC), Canada*

Use your device to scan and read the article online

Citation S. El Baakili, A. Semlali, K. El Mabrouk, M. Bricha. **Synthesis Method Effect on Acellular Bioactivity of Bioglasses: Structural Analysis and Solid-State NMR.** *J. Appl. Organomet. Chem.*, **2023**, *3*(4), 268-283.

https://doi.org/10.48309/JAOC.2023.416016.1117

Article info:
Received: 11 September 2023
Accepted: 02 October 2023
Available Online: 02 October 2023
ID: JAOC-2309-1117
Checked for Plagiarism: Yes
Language Editor checked: Yes

Keywords:
Structural properties, Bioglass, Solid-state NMR, Sol-gel, Hydrothermal, Bioactivity

ABSTRACT

This study used sol-gel and hydrothermal methods to prepare binary bioactive glasses (BG) of SiO_2-CaO with 63% and 37% molar fractions, respectively. Different techniques characterized heat-treated powders: Thermogravimetric analysis (TGA), Fourier-transformed infrared spectroscopy (FTIR), X-ray diffraction (XRD) analysis, inductively coupled plasma-atomic emission analysis (ICP-AES), solid-state nuclear magnetic resonance (NMR), scanning electron microscopy and energy dispersive spectroscopy (SEM-EDS), and Brunauer-Emmett-Teller analysis (BET). According to both synthetic routes, the HT technique presented better new apatite layers deposition on BG particles during in vitro bioactivity assessment in simulated body fluid (SBF). The bioactivity is confirmed by XRD analysis, NMR spectroscopy, and BET analysis showing that HT-derived bioactive glass (BG-HT) presents higher bioactivity than sol-gel-derived BG (BG-SG), and the nanometric particle size of HT-BG (90-100 nm) with a high specific surface area is responsible for this enhancement. Furthermore, NMR spectroscopy indicates the higher network connectivity of HT-derived bioactive glass due to different environments in this structure. Moreover, SEM-EDS micrographs of BG-HT glasses show spherical nanoparticles, while BG-SG results present a mixture of spherical and rod-like microparticles. The HT-BG could be a promising material for biomedical applications, especially in drug delivery and ion release.

Introduction

Bioactive glasses (BG) are successfully used in many applications to supplement or replace damaged tissue [1]. Furthermore, owing to their specific biodegradability and controllable bioactivity, these biomaterials are usually used in soft and hard tissue engineering to improve tissue regeneration [2,3].

For instance, in all cases of bone defects and pathologies (osteoporosis), it is crucial to rebuild the bone tissue in parallel with structure replacement and limit the degradation of bone tissue by stimulating osteoblast cells. Hence, bioactive glasses have

**Corresponding Authors: Meriame Bricha* (m.bricha@ueuromed.org)

received considerable attention for all these applications due to their ability to chemically react with biological fluid and produce a new apatite layer to promote bone growth.

The first prominent oxide glass, 45S5 bioactive, was synthesized by Professor L. Hench *et al.* in 1969. It was prepared based on SiO_2, P_2O_5, Na_2O, and CaO. The first two elements, considered formers, contribute to the cohesion of glass network. The others are network modifiers. They introduce the chain breaks and ensure the structural disorder. Their presence consequently affects the glass reactivity, which allows the formation of an apatite phase during the immersion in the physiological medium, and then stimulates the bone tissue [3-5].

Since their discovery, bioactive glass has been developed for different fields, especially incorporating several ions and drugs [6,7]. The composition of bioactive glass has been optimized to promote osteoblast proliferation and bone ingrowth [8,9]. Each incorporated element affects the behavior and properties of the glass, particularly on the glass dissolution or ion release [10,11]. The bioactive glass must have a controllable rate of dissolution to endure the progressive formation of hydroxyapatite and an extended-release of drugs [3]. However, these properties are related to the synthesis process of bioactive glass. Therefore, understanding the structure and the physicochemical behavior of bioglasses is a crucial step in developing new formulations of these bioglasses with enhanced properties.

The initial synthesis method of bioactive glass is a conventional melting-quench method [12]. In general, solid precursors are proportionally mixed, melted at a high temperature, and then cooled down rapidly to form glasses [13]. This process requires very high temperatures (typically around 1500 °C, depending on the chemical composition). Furthermore, it dramatically limits the porosity and specific surface area of the obtained powders [5], i.e. the aforementioned properties limit the contact surface between the bioactive glass and the physiological fluid. As known in the literature, when the specific surface area is more prominent, more is the bioactivity of glass powders [14]. The second method to produce bioglass is the sol-gel technique. It is one of the methods that mainly emerged by soft chemistry since 1990, in which precursors are mixed under liquid conditions (hydrolysis and polycondensation), followed by aging, drying, and calcination to form glasses [15]. During the last decades, different bioglass “BGs” with high textural characteristics (pore size, surface area, and pore volume) were synthesized by sol-gel-based self-assembly strategies involving surfactant as a template [16-19]. Despite the simplicity of the sol-gel method, producing spherical and monodisperse bioactive glass nanoparticles is not trivial. However, the drawbacks of bioglass produced by the sol-gel method are the size irregularity, polydispersity, and agglomeration of the particles [20].

Meanwhile, increasing research efforts are being invested by integrating the hydrothermal assisted process into the panoply of bioglass synthesis methods, even though it was just focused on the ceramic [21]. This leads to significant physicochemical properties of bioactive glass powders, like high purity, homogeneity, and controlled morphologies [22]. In addition, the hydrothermal method enhances the nucleation and drastically reduces the synthesis time and particle size of the produced glass powders [4,23]. Several bioglass synthesis strategies are available, but it should be noted that the effect of synthesis method varies based on the final goal, desired qualities, and the materials warranted. As a result, a thorough understanding of structure/network connectivity is required to tailor an efficient synthesis method to a specific composition and morphology. Therefore, the primary goal of this research is to investigate how the synthesis method influences the structural characteristics and *in vitro* bioactivity mechanism of glasses.

Accordingly, this article aims to study the impact of synthetic methods, sol-gel, and hydrothermal, on bioglasses' morphology and structural properties. In addition, different characterization techniques were used to approve the potential of these glasses to form bioactive layers on their surface; solid-state NMR spectroscopy and BET analysis were used to support the results of simulated body fluid in terms of fast and slow apatitic layer deposition on bioglasses particles and to confirm the

promising bioactive glass according to network connectivity and arrangement.

Experimental

Synthesis of 63S37C bioactive glass

Tetraethyl orthosilicate ($Si(OCH_2\ CH_3)_4$ TEOS ≥ 99%), calcium nitrate tetrahydrate ($Ca(NO_3)_2$ ≥ 99% $4H_2O$), cetyl trimethyl ammonium bromide ($C_{19}H_{42}BrN$, CTAB), ethanol, ammonia hydroxide (NH_4OH), and distilled water were used.

The desired glass chemical composition is $(SiO_2)_{0.63} - (CaO)_{0.37}$ (mol %). It was successfully synthesized by hydrothermal (BG-HT) and sol-gel (BG-SG) methods at 30 °C, using cetyl trimethyl ammonium bromide (CTAB) as a surfactant. The synthesis was performed according to the procedures described elsewhere with slight modifications [4,18]. The surfactant was initially dissolved in 120 ml of distilled water and ethanol for both methods, and then ammonium hydroxide was added as a catalyst. Afterward, proper amounts of ($Ca(NO_3)_2$, $4H_2O$) were added to the mixture depending on the glass composition, followed by continuous stirring for 30 minutes, and then TEOS was added dropwise. For the resulting gel-based produced by the sol-gel method, the mixture was allowed to react for an additional 4 hours, and then filtered and washed with distilled water. After that, the product was dried for one day at 80 °C, and then sintered at 600 °C for 6 hours. However, for the hydrothermal process, the resulting gel-based was mixed for 30 min, then the white precipitate was put in a Teflon-lined stainless autoclave and heated at 150 °C for 24 hours. The final product was dried for one day at 80 °C, and then sintered at 700 °C for 6 hours.

Structural characterization

Solid-state nuclear magnetic resonance (NMR)

NMR analysis was performed on sintered powders of BG-SG and BG-HT-derived samples. A powder of each BG specimen was packed in a 3.2 mm zirconia rotor and underwent MAS rate of ωr = 19 kHz for all acquisitions. All magic-angle spinning (MAS) NMR experimentation was realized at 14 T with a Jeol (JNM-ECZR series) spectrometer at a magnetic field operating at 600.1 MHZ for ^{1}H and 119.24 MHZ for ^{29}Si, respectively.

The relaxation delays were adapted for each sample based on separate spin-lattice relaxation measurements. The NMR spectra produced by these experimental conditions quantitatively reflect each silicate component in the structure.

Thermogravimetric analysis (TGA)

A Thermogravimetric Analysis (TGA) characterized the glass's thermal behavior using a Q500-TA Instrument apparatus. TGA thermograms were obtained by heating the samples from room temperature to 1000 °C at a heating rate of 10 °C/min^{-1} under a constant flow of air atmosphere.

The elemental analysis (ICP-AES)

The synthesized samples were analyzed using inductively coupled plasma-atomic emission spectroscopy "ICP-AES; JobinYvon Horiba-Ultima 2 apparatus". The measurements were repeated three times, and the results section represents the average.

X-ray diffraction (XRD)

XRD identification was performed by X-ray Diffraction (XRD) analysis with an automated X-ray powder diffractometer (Panalytical) using CuKα radiation at a voltage and current of 45 kV and 40 mA, respectively.

Fourier transformed infrared spectroscopy (FTIR)

A Fourier Transformed Infrared Spectroscopy determined the chemical bonding groups in Attenuated Total Reflection mode (FTIR-ATR) by an "IS50 spectrometer". The samples were analyzed in a total of 32 iterations in the range of 400 to 4000 cm^{-1} with a resolution of 4 cm^{-1}.

Scanning electron microscopy coupled energy dispersive X-ray spectroscopy (SEM-EDS)

QUATTRO environmental scanning electron microscope (ESEM-FEG, ThermoFisher

Table 1. Ion concentration (mM/l) in SBF and human blood plasma [4,21,24]

Ion	Na^+	K^+	Mg^{2+}	Ca^{2+}	Cl^-	SO_4^-	HCO_3^-	HPO_4^{2-}
Plasma	142	5	1.5	2.5	103	0.5	27	1
SBF	142	5	1.5	2.5	147.8	0.5	4,2	1

Scientific, USA) was used to characterize the samples' morphology under a high vacuum, and then the images were analyzed with ImageJ software (National Institute of Health, USA).

Nitrogen adsorption-desorption isotherm and texture properties (BET)

Textural properties were determined using N_2 adsorption/ desorption isotherms analysis using TriStar II plus from micrometric.
The analysis was performed at 77.300K, with a degassing before the measurement at 100 °C for 12 h to remove moisture and contaminants from the surface. Brunauer–Emmett–Teller (BET) method allows calculating the total pore volume from the amount of N_2 adsorbed at a relative pressure of 0.995, corresponding to complete pore filling, and the pore size distribution was obtained using the Barrett–Joyner–Halenda (BJH) method.

In vitro bioactivity in an acellular medium

According to Kokubo's method [24], the acellular test was performed. Initially, the glass samples were soaked in simulated body fluid (SBF). SBF is a synthetic solution with a similar ionic concentration to human blood plasma (**Table 1**); in sterilized bottles for different periods from 3 hours to 14 days [4]. The powder ratio to the solution was 2:1 (mg/ml), and the bottles were incubated at 37.0 °C. After each selected period, the pH was measured via a pH meter (Seven Compact pH/Ion meter - pH METTLER TOLEDO), and then the powders were collected by filtration, washed with distilled water, and dried at 40 °C for 24 h. Moreover, the prepared samples were compared using different technics (FTIR, XRD, and SEM-EDX) to determine their ability to form apatite [25,26].

Results and Discussion

Structural analysis

As well-known in the literature, the amorphous structure of the glasses is a natural consequence of a random atoms arrangement and three-dimensional network lacking symmetry and periodicity [27].

The fundamental unit of silicate-based glasses is the SiO_4 tetrahedron. To construct a 3D network structure, this unit can share up to four oxygen atoms with other tetrahedral units [28]. The tetrahedral silicate network former establishes an aperiodic network of coordination tetrahedra, noted $Q^{(n)}_X$ species, n is the number of bridging oxygen atoms (BO), and X represents ions that charge-balance non-bridging oxygen atoms (NBO) whose number is '4 – n' per silicate tetrahedra [29]. These species reflect the silicon environment depending on the non-bridging oxygens (NBO) the atom is bound, revealing the potential network connectivity and glass bioactivity. Furthermore, when the glass bioactivity is very high, it means it contains an increased number of NBO ($Q^{(2)}$, $Q^{(3)}$) linked to network modifiers or highly interconnected glass with a high number of $Q^{(4)}$. For instance, $Q^{(4)}$ corresponds to a silicon atom linked to four (OSi) groups, and $Q^{(3)}$ corresponds to a silicon atom attached to three (OSi) groups, an NBO, and son forth [30].

This study uses single-pulse-acquired MAS ^{29}Si solid-state NMR spectroscopy (**Figure 1**) as a chemical characterization to evaluate the bioactivity and network connectivity of the selected BG-SG and BG-HT to identify the best candidate to interact with physiological fluid. As is noticed below, different fractional populations are obtained after deconvoluting the spectrum. Hence, BG-SG presents a strong influence on the type of silicon-oxygen

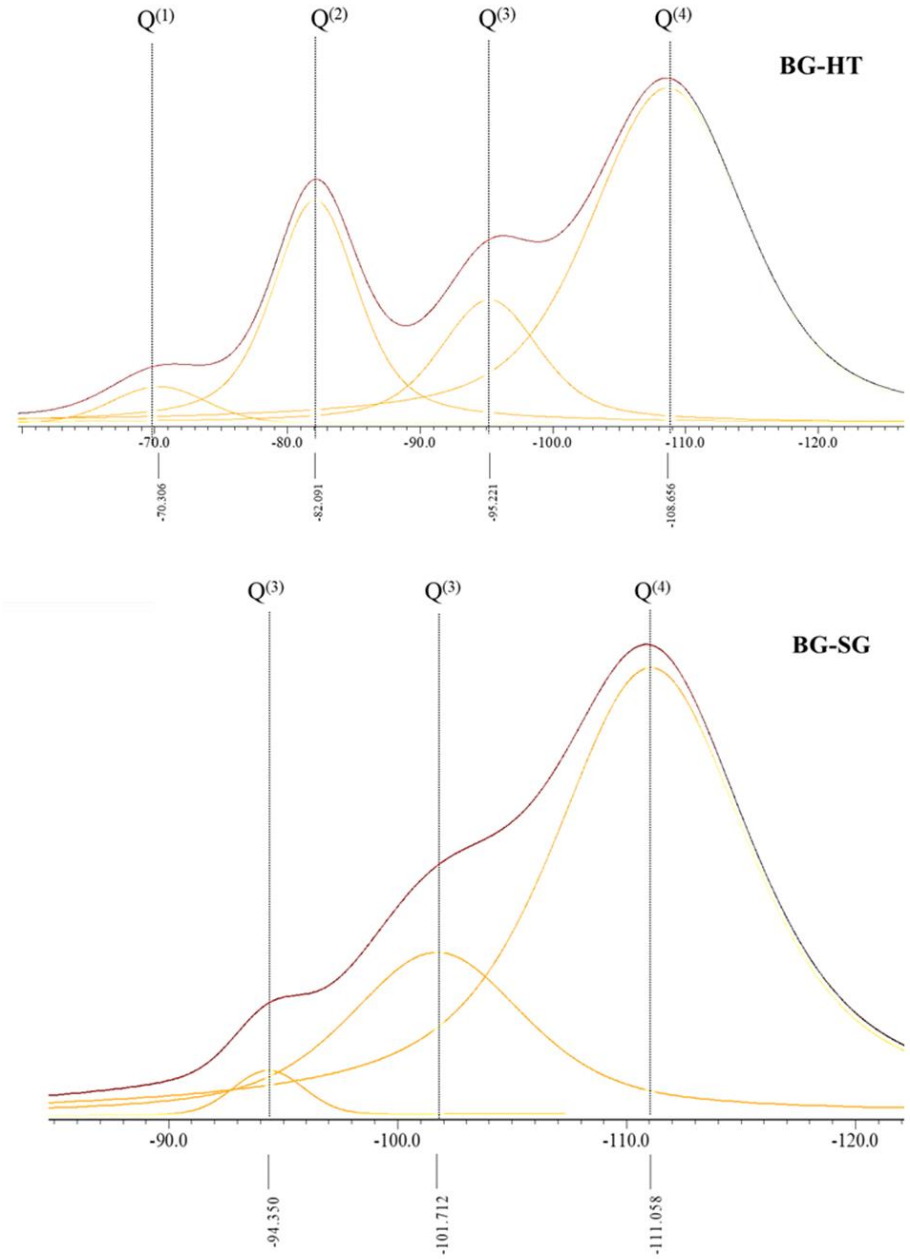

Figure 1. ^{29}Si MAS-NMR spectra for derived glass

tetrahedron, with chemical shifts appearing at -111 ppm for $Q^{(4)}$, -101 for $Q^{(3)}_{H}$, and $Q^{(3)}_{Ca}$ at -94 ppm, compared to previously described values for other BGs in the literature [31,32]. These results correspond to a silicon network with a more elevated polymerization level [10]. However, BG-HT presents major environments $Q^{(4)}$, $Q^{(3)}_{Ca}$, $Q^{(2)}_{Ca}$, $Q^{(3)}_{Ca}$, and $Q^{(1)}_{Ca}$, appearing at -109 ppm, -95 ppm, -82 ppm, -69 ppm, respectively, This result indicate that BG-HT compromise larger amount of networks modifiers, thereby exhibiting more open network than sol-gel glass for the same composition. Likewise, this structure will make it easier to release network modifiers like calcium to the body medium and take hydrogen

Table 2. Deconvolution results of the ^{29}Si MAS NMR spectra obtained by single-pulse excitation

Acronym	BG-HT			BG-SG		
Parameters	δ (ppm)	Fwhm (ppm)	Fraction (%)	-δ (ppm)*	Fwhm[a] (ppm)	Fraction[b] (%)
$Q^{(1)}_{Ca}$	70.305	9.926	5.029	-	-	-
$Q^{(2)}_{Ca}$	82.090	8.485	31.086	-	-	-
$Q^{(3)}_{Ca}$	95.221	9.963	17.154	94.349	4.340	6.783
$Q^{(3)}_{H}$	-	-	-	101.711	10.201	24.840
$Q^{(4)}$	108.655	15.502	46.729	111.058	11.1394	68.375
NC[c]		3.055			3.683	

* Chemical shifts; [a] Full width at half-maximum height, [b] fractional population, and [c] network connectivity

Table 3. Weight losses at different temperatures for BG-SG and BG-HT

Sample	Weight loss (%)		
	I (50-190 °C)	II (200-450 °C)	III (500-800 °C)
BG-SG	7.7	17.08	2.19
BG-HT	5.95	8.37	1.16

to form silanol groups. Despite that, it facilitates the first stage of bioactivity [29].

Table 2 presents the contribution of each environment in the structure network of BGs. For example, BG-HT possesses almost 47% (**Table 2**) contribution of the $Q^{(4)}$, while the $Q^{(2)}$ was equivalent to 32 % for Ca and 17% for proton units since the signal separation between members of each group of $Q^{(n)}$ Ca and $Q^{(n)}$ proton units is proportional to their peak widths. Furthermore, the mean chemical shifts of the $Q^{(2)}_{H}$ and $Q^{(3)}_{Ca}$ species are nearly equal [29]. Nevertheless, for sol-gel-derived glass, the contribution of $Q^{(4)}$ and $Q^{(2)}$ were 68 % and 7 %, respectively. Hence, the high participation of the $Q^{(4)}$ environment indicates an excessive number of NBO and less bioactive glass with increased connectivity. The peak shapes and full width reflect this difference in the two structures at half maximum (FWHM) (**Table 2**) [31]. As a result, this funding will be confirmed by the XRD, FTIR, and SEM results displayed below since it reveals the effect of the synthesis method on the network structure and bioactivity behavior. Hydrothermal synthesis seems more convenient for producing a highly bioactive glass without counterbalancing the network connectivity.

The TGA curves at the heating rate of 10 °C/min for the as-dried bioactive glass powders synthesized with a CTAB as the template are depicted in (**Figure 2**(a)). The total weight loss between 20-1000 °C is about 16 % and 27% for BG-HT and BG-SG, respectively. The TGA result showed three mass losses for both BGs (**Table 3**): the desorption of physically adsorbed water molecules was at about 50-190 °C (I) [2,4], and the subsequent loss of the residual CTAB, nitrate, and ethanol were between 200-450 °C (II). The last interval, from 500 to 800 °C (III), is related to the crystallization of bioactive glass.

Figure 2(a) shows no mass loss was observed from temperatures above 600 °C for BG-SG. Therefore, the obtained powders were thermally treated at 600 °C for BG-SG, and 700 °C was selected for BG-HT to get a pure and stable glass.

The XRD patterns of BG-SG and BG-HT bioactive glass are demonstrated in **Figure 2(b)**. After calcination, the synthesized compositions exhibited a broad peak between 20 º and 30 º (2θ). This band characterizes a completely amorphous silicate, which indicates an entirely amorphous structure. This observation specifies the absence of any crystalline phase and the presence of an amorphous structure characteristic of the glassy phase. These results are consistent with our previous study [4], and the same results were obtained by Martínez A *et al.* [33], Ta Anh Tuan *et al.* [34], and Bui Thi Hoa *et al.* [35] in their synthesis of the binary 70S30C by hydrothermal and sol-gel processes. However, the XRD patterns reveal a slight difference in the intensity of the peaks, where the BG-HT presents a higher intensity than BG-SG, probably due to the higher speed of the arrangement at high pressure and temperature

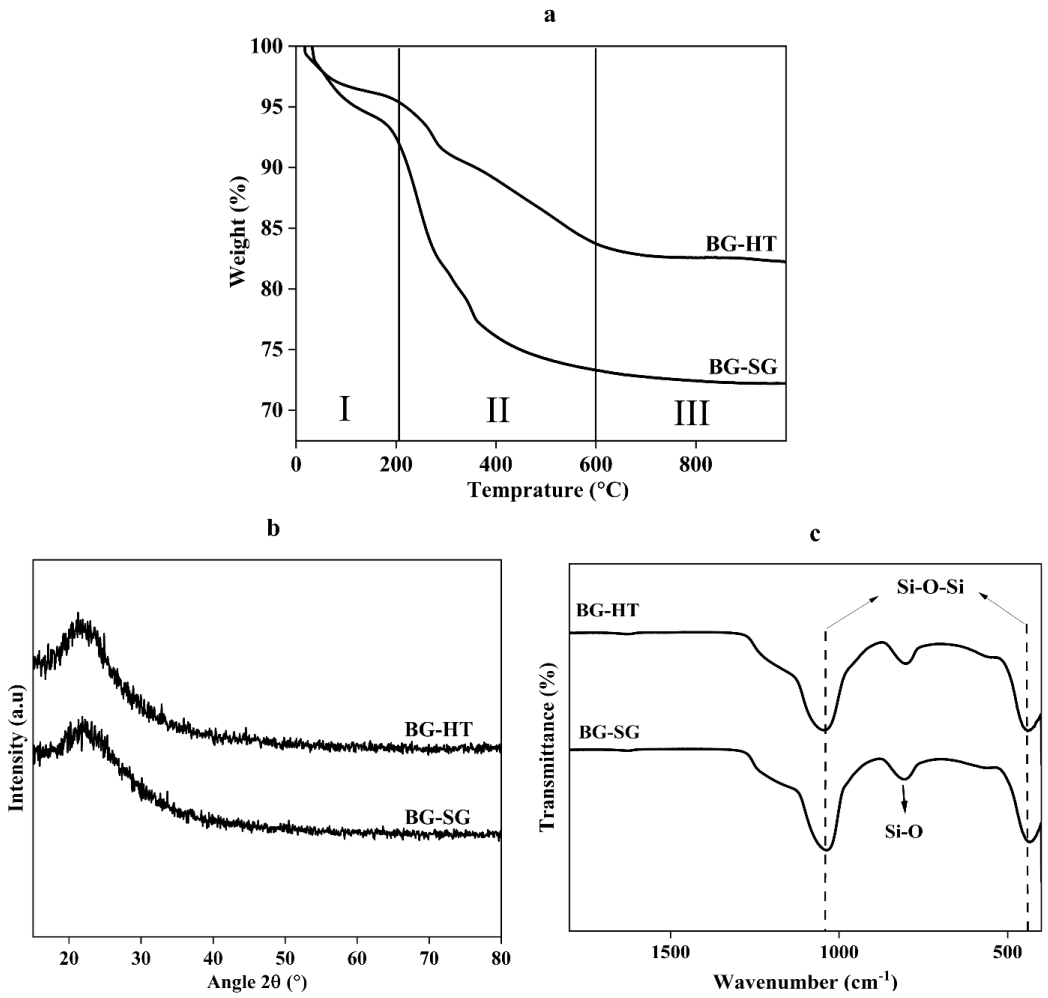

Figure 2. (a) TGA spectra, (b) XRD patterns, and (c) FTIR spectra of calcined BG-SG and BG-HT

of the network. Accordingly, sol-gel and hydrothermal methods can produce powders characterized by glass properties without any crystallized phase.

The structural characterization has been completed with the FTIR analysis. The spectra of the two silicate materials after calcination are illustrated in (**Figure 2(c)**). The results showed identical bending for both bioactive glasses, the bending, and stretching vibrations assigned to the silica network existing in bioactive glasses (439, 807, and 1035 cm^{-1}) [36-38]. A band at 439 cm^{-1} refers to the rocking vibration of the Si–O–Si bending mode. The second band at 807 cm^{-1} was assigned to the symmetric stretching vibration of Si–O. This is related to the stretching vibration of Si-OH bonds, indicating the increased network connectivity and the formation of more bridging oxygen. The third band at around 1035 cm^{-1} refers to the Si–O–Si asymmetric stretching mode. The results are compatible with the bioactive glass presented in the literature [4, 18, 28]. Usually, in the presence of certain NBOs, the SiO absorption frequency often falls between 1030 and 800 cm^{-1}. Most SiO_4 groups contain at least some NBOs [39]. This finding agrees with NMR results in terms of connectivity.

Elemental analysis ICP-AES

Table 4 summarizes the elementary composition of prepared powders measured by ICP-OES. The molar percentages of oxides are expressed according to ICP-OES elemental analysis. Based on **Table 4**, it observed a slight shift in the nominal compositions. Overall,

Table 4. Molar composition by ICP-AES

Sample acronym	SiO_2 % mol	CaO % mol
BG-SG	61.08 ± 0.05	35.09 ± 0.03
BG-HT	62.08 ± 0.04	36.52 ± 0.06

these results suggest the success of hydrothermal and sol-gel methods in glass synthesis, with a little difference. This might be due to the heterogeneous distribution of the elements on the amorphous glass matrix.

Scanning electronic microscopy-coupled energy dispersive X-ray spectroscopy (SEM-EDS)

SEM micrographs of as-sintered BG-HT and BG-SG powders are depicted in **Figure 3**. As can be seen, BG-SG (**Figure 3b**) are irregular in shape (rod-like and spheric), non-uniform, and not homogeneous. Size distribution was also obtained, consisting of microparticles in the range of 29-30 µm. However, BG-HT (**Figure 3a**) shows aggregations with a homogeneous morphology (small spherical particles). It is crucial to mention that producing well-dispersed BG particles less than 100 nm is challenging since smaller particles are more likely to agglomerate [4]. Indeed, for the BG-HT sample, particle size is in the range of 90-100 nm, therefore, by providing a large surface area for ion exchange, BG-HT nanoparticles are promising for biomedical applications and drug delivery [40].

SEM micrographs demonstrate that the hydrothermal process leads to small particles of uniform size. The above results agree with the morphology theory and are controlled by the process conditions, which is confirmed by Qiming Liang *et al.*, who studied the effect of a novel sacrificial liquid template method in the sol-gel process on particle morphology [22]. Furthermore, the same finding agrees with previous studies' results where non-porous particles and monodispersed spherical nanoparticles were produced via the Stöber method [41, 42].

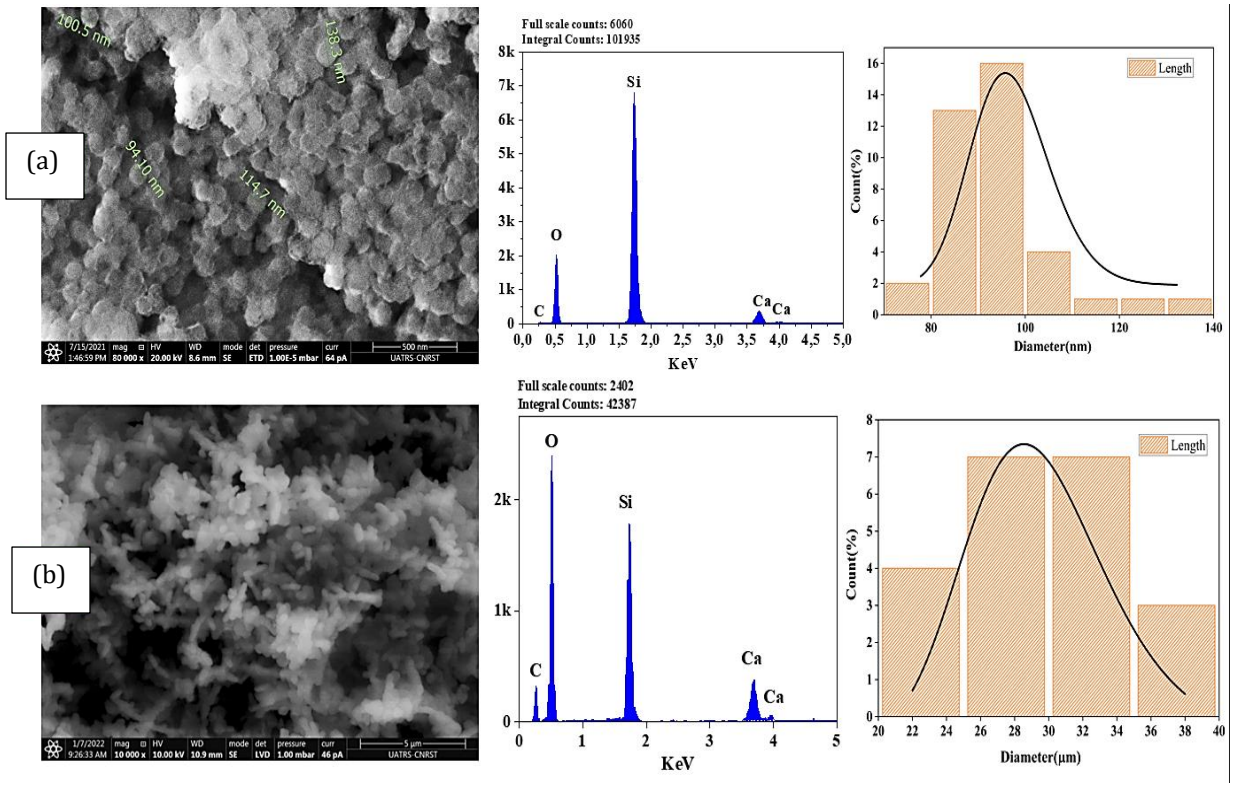

Figure 3. SEM-EDS analyses and particle size distribution of calcined bioactive glass: (a) BG-HT, (b) BG-SG

Table 5. Textural properties of the examined glasses

Composition	Surface area $m^2.g^{-1}$	Total pore volume $cm^3\ g^{-1}$	Average pore size nm
BG-SG	19.7005 ± 0.2090	0.001678	7.8905
BG-HT	33.7238 ± 0.1385	0.000911	19.3563

Textural properties (BET)

A material's specific surface area can be determined using the BET (Brunauer-Emmett-Teller) analysis, which can reveal details about the textural characteristics of bioactive glass. For example, a high specific surface area is a sign of high porosity.

The synthesis process significantly influences the textural characteristics of bioactive glass. For instance, compared to the melt-quench method, the sol-gel method may produce a more homogeneous, porous structure with a higher specific surface area [19]. On the other hand, the melt-quench technique makes a structure with a smaller specific surface area but more compact and dense [43]. Therefore, the bioactivity and effectiveness of bioactive glass in various applications can be impacted by the synthesis method choice [44]. Similarly, a porous surface can provide nucleation sites for apatite formation, while a dense surface may inhibit it.

In this study, the hydrothermal exhibits high surface area than Sol-gel method (**Table 5**), indicating mesoporosity of almost 20 nm. The presence of adsorption/desorption hysteresis (**Figure 4**) confirms the mesoporosity for both examined bioactive glasses. Moreover, BG-SG and BG-HT show different hysteresis loops, a larger hysteresis loop for BG-HT shows a more porous surface, while the smaller one suggests a smother surface with less porosity[45].

According to the calculations and hysteresis loops, the surface area increases with the hydrothermal process, which confirms the NMR results, showing that BG-HT is more bioactive and provides further nucleation sites for apatite formation more than sol-gel bioactive glasses.

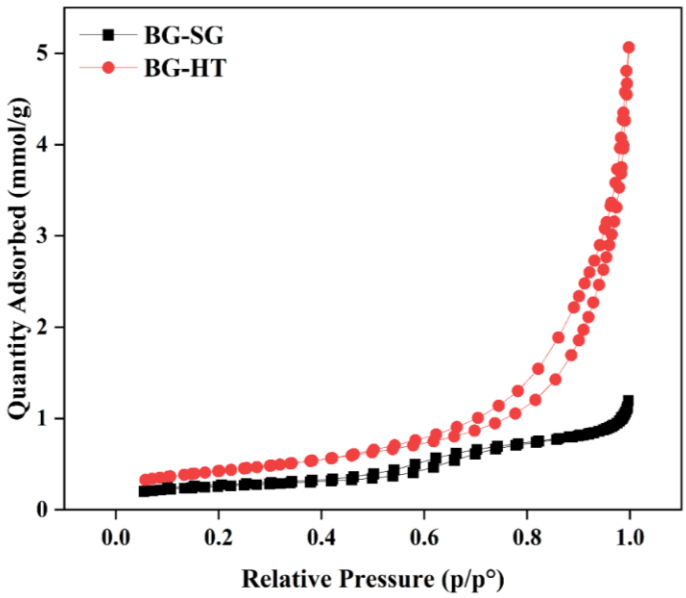

Figure 4. N_2 adsorption-desorption isotherms for both studied glasses

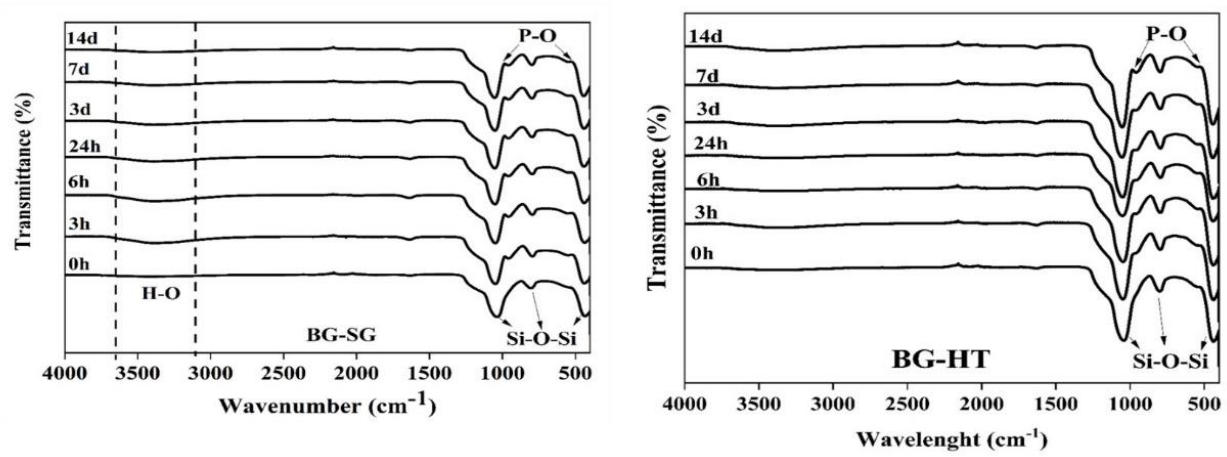

Figure 5. FTIR spectra of BG-SG and BG-HT after immersion in SBF

In-vitro acellular test evaluation

Bioactivity can induce apatite layer formation through ionic exchanges with physiologic fluid. FTIR, XRD analysis, and MEB-EDS spectroscopy generally confirm this bioactivity. For example, in **Figure 5**, peaks appeared in the range of (557-630 cm^{-1}), and around 984 cm^{-1} shows the bending vibrations of P–O related to the presence of amorphous apatite [26, 46]. The intensity of the peaks is higher in BG-HT, revealing higher crystalline apatite formation on the glass surface. Furthermore, after different periods of soaking, it is noticed that apatite deposition increases with a longer time. This finding agrees with the Wei-Hua Lu *et al.* study, indicating a dense apatite layer with extended immersion time [47].

FTIR analysis shows that the apatite deposition increases while the soaking time is extended. Hence, 14 days was chosen as a period of immersion to be presented for XRD. These results are confirmed with XRD spectra (**Figure 6(a)**).

XRD patterns show a starting crystallinity phase for BG-HT, with the main peak of the HA phase [48] at 25° and 32° showing the (002) and (211) reflections. However, BG-SG presents only one slight peak at 32° relative to the plan (211). It is worth noting that BG-HT shows interesting bioactivity marked by the formation of an apatite phase after immersion in SBF for 14 days. Moreover, it finds potential applications better than BG-SG bioglass. Previous studies obtained similar results for binary bioactive glass (70S30C) synthesized by the conventional sol-gel and found that, after SBF immersion, the mineral apatite is formed at well-defined peaks at about 26° and 32° [33, 34, 49].

FTIR, XRD, pH, and SEM analysis evaluate the *in vitro* bioactivities. Therefore, changes in pH behavior during SBF immersion are crucial to confirm the apatite layer formation.

The results of pH measurement in 0, 3 hours, and 1, 3, 7, and 14 days are shown in (**Figure 6(b)**). As can be observed, the samples had nearly identical pH variation patterns, with an increased value until the end of the test (14 days, from the initial range of 7.4 to 7.99 and 8.03 for BG-SG and BG-HT, respectively).

Rapid dissolution of the glass surface happens during the first few hours of the test, accompanied by an ionic exchange between the Ca^{2+} of the glass and the H^+ ions present in the SBF. The pH values of SBF increase over incubation time, which is related to the bioactive glasses' partial dissolution and surface reactivity. According to Professor L.L. Hench [5], this phenomenon can be explained in five steps: ion exchange occurs when H^+ from the medium initially replaces Ca^{2+} and Na^+ cations in the glass. This ionic exchange leads the silicon network to break down, forming $Si(OH)_4$ on the bioactive glasses' surface. In the

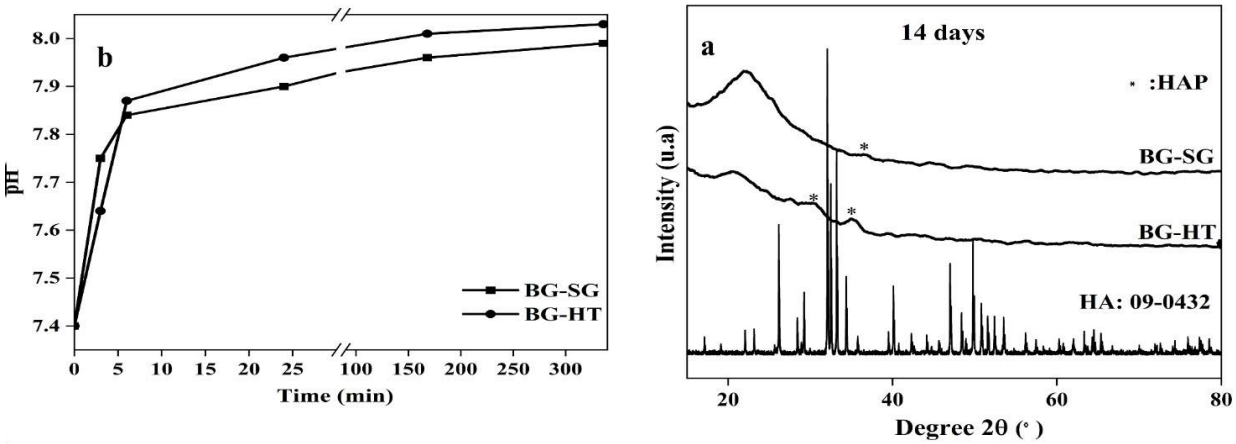

Figure 6. (a) XRD patterns of BG-SG and BG-HT after SBF medium immersion for 14 days, and (b) pH variations during the bioactivity tests in SBF of the BG-SG and BG-HT samples

next phase, silicic acid dissolves and depolymerizes, creating a generous silica gel layer on the glass surface (third step). In the fourth step, incorporating Ca^{2+} and PO_4^{3-} ions into the silica gel layer creates an amorphous calcium phosphate surface layer. After incorporating CO_3^{2-} anions from the medium, HA crystallizes in the final phase.

It can be summarized that the *in vitro* study of the two prepared glasses allows good bioactivity enhancement. Therefore, we can consider these two glasses as bioactive because they react chemically with physiological fluids (SBF), enabling the growth of a phase similar to the mineral component of the bone. The other authors have confirmed this result about the bioactivity of different sol-gel-derived binary glasses systems [49].

SEM-EDX analysis was performed on the powders after 14 days of immersion in the SBF medium to support the previous finding. **Figure 7** shows the SEM-EDX micrographs. The formation of a new apatite was identified by a new layer covering all the glass surfaces after SBF immersion. SEM micrographs (**Figure 7(a)**) indicate nanocrystalline apatite on the BG-HT surface, with a needle-like shape.

Interestingly, the EDX result confirms the presence of phosphorus in the composition of both bioactive glasses (**Figure 7**), supported by a steady drop in the silicon "Si" peaks over the 14-day immersion period, as the soluble SiO_2 was lost from the surface of the glass specimens to the SBF solution. This is in concordance with FTIR and XRD results. For instance, the intensity of phosphorus peak after soaking in SBF solution is evident in both samples. This indicates the tendency to form Ca-P apatite layer on the glass surface, as proved by XRD results (**Figure 6(a)**). This finding was confirmed by the studies of M. Vallet-Regi and A. Martinez [49].

According to elementary composition (EDS), the Ca/P ratio obtained in the compositions considered in this study is equal to 1.66 and 1.63 for BG-HT and BG-SG, respectively (**Table 6**), which is near to the existing one in human bone structure. This finding agrees with the study of U Tariq *et al.* [50,51].

Table 6. Results of calculation of Ca/P ratio based on EDX analysis after 14 days soaking in SBF

BG-HT	Atom %	EDX Ca/P ratio	BG-SG	Atom %	EDX Ca/P ratio
C K	9.42	1.666	C K	14.46	1.639
O K	62.49		O K	60.41	
Si K	26.33		Si K	23.52	
P K	0.66		P K	0.61	
Ca K	1.10		Ca K	1.00	
	100.00			100.00	

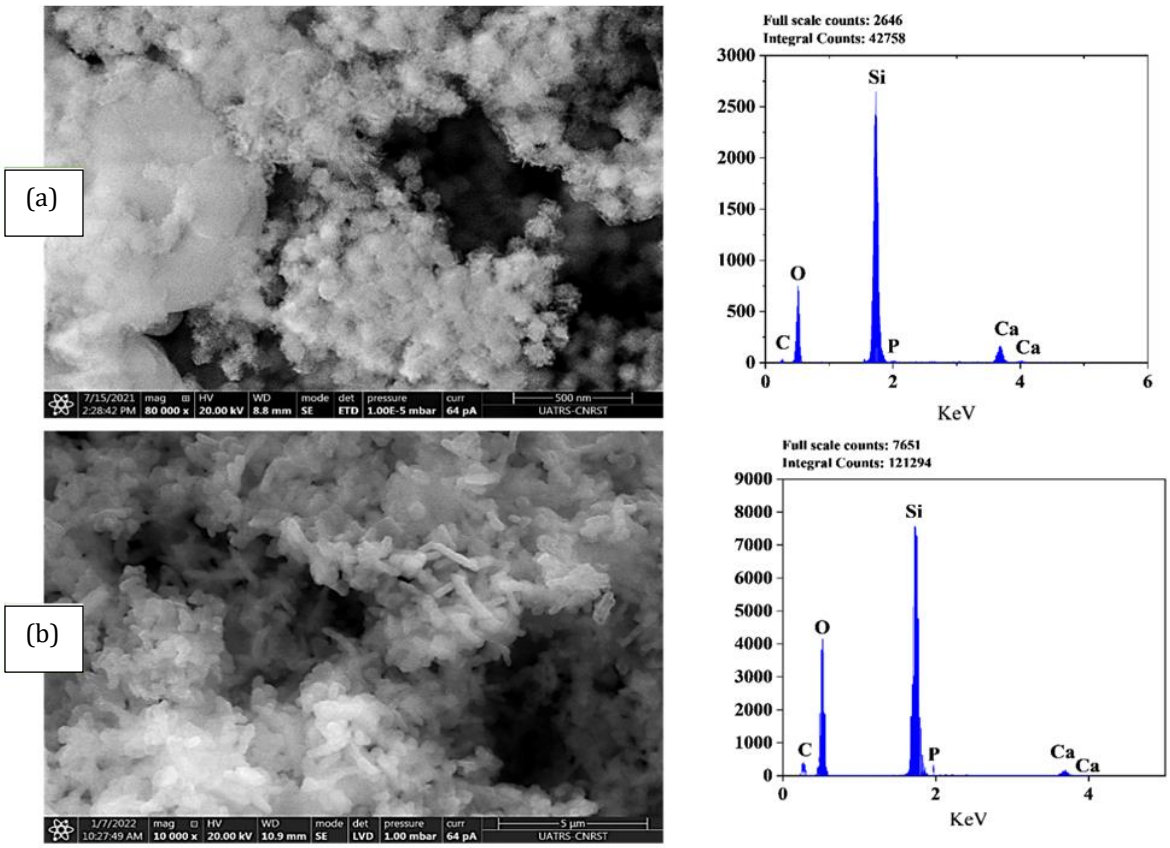

Figure 7. EDX-SEM images of bioactive glasses after immersion in SBF for 14 days: (A) BG-HT and (B) BG-SG

Conclusion

The bioactive glass "63S37C" was successfully synthesized by hydrothermal and sol-gel methods. The structural and chemical compositions were ensured from the analytical results (Solid-state NMR, XRD, BET, FTIR, ICP-AES, and SEM-EDX). For instance, according to NMR analysis, the contribution of different environments in the BG-HT network indicates higher network connectivity and high bioactivity of this glass. Similarly, BET method confirms the high surface area of BG-HT, which shows high bioactivity compared to BG-SG. In addition, the *in vitro* study confirms the growth of new crystallized apatite layers on the surface of particles prepared by both methods. Likewise, FTIR and XRD were performed to prove the ability of 63S37C bioactive glasses to form an apatite layer on their surface. Hence, after 14 days of immersion in SBF, BG-HT exhibits intriguing bioactivity by forming a Ca-P layer. Furthermore, it finds more possible applications than BG-SG bioglass.

The hydrothermal synthesis displayed rapid apatite formation more than the sol-gel method. Moreover, the hydrothermal method allows the construction of an amorphous phase of bioglass, with enhanced bioactivity in an acellular medium, within 14 days.

Orcids

Salwa El Baakili
https://orcid.org/0000-0001-8616-9111

Abdelhabib Semlali
https://orcid.org/0000-0002-1643-0377

Khalil El Mabrouk
https://orcid.org/0000-0002-7097-0737

Meriame Bricha
https://orcid.org/0000-0002-3073-8845

Acknowledgements

The authors acknowledge funding from the Euromed University of Fes and Laval University, Quebec City (QC), Canada.

Conflict of interest

The authors declare that there are no conflicts to declare.

References

[1]. V. Miguez-Pacheco, L.L. Hench, A.R. Boccaccini, Bioactive glasses beyond bone and teeth: Emerging applications in contact with soft tissues, *Acta Biomater*, **2015**, *13*, 1-15. [Crossref], [Google Scholar], [Publisher]

[2]. P. Saravanapavan, L.L. Hench, Mesoporous calcium silicate glasses. I. Synthesis, *Journal of Non-Crystalline Solids*, **2003**, *318*, 1-13. [Crossref], [Google Scholar], [Publisher]

[3]. A.T. Contreras Jaimes, G. Poologasundarampillai, D.S. Brauer, Bioactive glasses, Kirk-Othmer encyclopedia of chemical technology, **2019**, 1-41. [Crossref], [Google Scholar], [Publisher]

[4]. a) S.El. Baakili, K.El. Mabrouk, Acellular bioactivity and drug delivery of new strontium doped bioactive glasses prepared through a hydrothermal process, *RSC Advances*, **2022**, *12*, 15361-15372. [Crossref], [Google Scholar], [Publisher] b) H.A. Ameer Radhi, M. Abdulaziz Ahmad, Biological test of porous geopolymer as a bone substitute, *Journal of Medicinal and Chemical Sciences*, **2023**, *6*, 710-719. [Crossref], [Google Scholar], [Publisher]

[5]. L.L. Hench, The story of bioglass®, *Journal of Materials Science: Materials in Medicine*, **2006**, *17*, 967-978. [Crossref], [Google Scholar], [Publisher]

[6]. a) N. Gupta, D. Santhiya, S. Murugavel, A. Kumar, A. Aditya, M. Ganguli, S. Gupta, Effects of transition metal ion dopants (Ag, Cu, and Fe) on the structural, mechanical and antibacterial properties of bioactive glass, *Colloids and Surfaces A: Physicochemical and Engineering Aspects*, **2018**, *538*, 393-403 [Crossref], [Google Scholar], [Publisher] b) O. Daliri Shamsabadi, Investigation of antimicrobial effect and mechanical properties of modified starch films, cellulose nanofibers, and citrus essential oils by disk diffusion method, *Asian Journal of Green Chemistry*, **2024**, *8*, 1-14. [Crossref], [Publisher]

[7]. A. Bachar, R. Catteaux, C. Duée, F. Désanglois, I. Lebecq, C. Mercier, C. Follet-Houttemane, Synthesis and characterization of doped bioactive glasses, *Biomedical, Therapeutic and Clinical Applications of Bioactive Glasses*, **2019**, 69-123. [Crossref], [Google Scholar], [Publisher]

[8]. F. Kermani, S.M. Beidokhti, F. Baino, Z. Gholamzadeh-Virany, M. Mozafari, S. Kargozar, Strontium-and cobalt-doped multicomponent mesoporous bioactive glasses (MBGS) for potential use in bone tissue engineering applications, *Materials*, **2020**, *13*, 1348. [Crossref], [Google Scholar], [Publisher]

[9]. Z. Neščáková, K. Zheng, L. Liverani, Q. Nawaz, D. Galusková, H. Kaňková, M. Michálek, D. Galusek, A.R. Boccaccini, Multifunctional zinc ion doped sol-gel derived mesoporous bioactive glass nanoparticles for biomedical applications, *Bioactive Materials*, **2019**, *4*, 312-321. [Crossref], [Google Scholar], [Publisher]

[10]. X. Kesse, C. Vichery, A. Jacobs, S. Descamps, J.M. Nedelec, Unravelling the impact of calcium content on the bioactivity of sol-gel-derived bioactive glass nanoparticles, *ACS Applied Bio Materials*, **2020**, *3*, 1312-1320. [Crossref], [Google Scholar], [Publisher]

[11]. Á.J. Leite, A.I. Gonçalves, M.T. Rodrigues, M.E. Gomes, J.F. Mano, Strontium-doped bioactive glass nanoparticles in osteogenic commitment, *ACS Applied Materials & Interfaces*, **2018**, *10*, 23311-23320. [Crossref], [Google Scholar], [Publisher]

[12]. J.R. Jones, Reprint of: Review of bioactive glass: From Hench to hybrids, *Acta Biomaterialia*, **2015**, *23*, S53-S82. [Crossref], [Google Scholar], [Publisher]

[13]. T. Mehrabi, A.S. Mesgar, Z. Mohammadi, Bioactive glasses: a promising therapeutic ion release strategy for enhancing wound healing, *ACS Biomaterials Science & Engineering*, **2020**, *6*, 5399-5430. [Crossref], [Google Scholar], [Publisher]

[14]. C. Vichery, J.-M. Nedelec, Bioactive glass nanoparticles: From synthesis to materials

design for biomedical applications, *Materials*, **2016**, *9*, 288. [Crossref], [Google Scholar], [Publisher]

[15]. R. Li, A.E. Clark, L.L. Hench, An investigation of bioactive glass powders by sol-gel processing, *Journal of Applied Biomaterials*, **1991**, *2*, 231-239. [Crossref], [Google Scholar], [Publisher]

[16]. M. Vallet-Regi, A. Rámila, R.P. del Real, J. Pérez-Pariente, A new property of MCM-41: drug delivery system, *Chemistry of Materials*, **2001**, *13*, 308-311. [Crossref], [Google Scholar], [Publisher]

[17]. A. Rámila, F. Balas, M. Vallet-Regí, Synthesis routes for bioactive sol-gel glasses: Alkoxides versus nitrates, *Chemistry of Materials*, **2002**, *14*, 542-548. [Crossref], [Google Scholar], [Publisher]

[18]. Z. Tabia, K. El Mabrouk, M. Bricha, K. Nouneh, Mesoporous bioactive glass nanoparticles doped with magnesium: drug delivery and acellular in vitro bioactivity, *RSC Advances*, **2019**, *9*, 12232-12246. [Crossref], [Google Scholar], [Publisher]

[19]. K. Deshmukh, T. Kovářík, T. Křenek, D. Docheva, T. Stich, J. Pola, Recent advances and future perspectives of sol-gel derived porous bioactive glasses: a review, *RSC Advances*, **2020**, *10*, 33782-33835. [Crossref], [Google Scholar], [Publisher]

[20]. F. Paquin, J. Rivnay, A. Salleo, N. Stingelin, C. Silva, Multi-phase semicrystalline microstructures drive exciton dissociation in neat plastic semiconductors, *Journal of Materials Chemistry C*, **2015**, *3*, 10715-10722. [Crossref], [Google Scholar], [Publisher]

[21]. a) M. Bricha, V. Nivedha, M. Ramadas, K.El. Mabrouk, A.M. Ballamurugan, Investigations on the influence of magnesium ion in the surfactant assisted hydrothermaly synthesized nanoscale hydroxyapatite, *Trends in Biomaterials & Artificial Organs*, **2018**, *32*, 1-9. [Crossref], [Google Scholar], [Publisher] b) M. Ahmadlouydarab, S. Javadi, F. Adel Alijan Darab, Evaluation of thermal stability of TiO_2 applied on the surface of a ceramic tile to eliminate methylene blue using silica-based doping materials, *Advanced Journal of Chemistry, Section A,* **2023**, *6*, 352-365. [Crossref], [Google Scholar], [Publisher]

[22]. Q. Liang, Q. Hu, G. Miao, B. Yuan, X. Chen, A facile synthesis of novel mesoporous bioactive glass nanoparticles with various morphologies and tunable mesostructure by sacrificial liquid template method, *Materials Letters*, **2015**, *148*, 45-49. [Crossref], [Google Scholar], [Publisher]

[23]. Y.X. Gan, A.H. Jayatissa, Z. Yu, X. Chen, M. Li, Hydrothermal synthesis of nanomaterials, *Journal of Nanomaterials*, **2020**, *2020*, 1-3. [Crossref], [Google Scholar], [Publisher]

[24]. T. Kokubo, H. Takadama, How useful is SBF in predicting in vivo bone bioactivity?, *Biomaterials*, **2006**, *27*, 2907-2715. [Crossref], [Google Scholar], [Publisher]

[25]. G. Rajkumar, V. Dhivya, S. Mahalaxmi, K. Rajkumar, G.K. Sathishkumar, R. Karpagam, Influence of fluoride for enhancing bioactivity onto phosphate based glasses, *Journal of Non-Crystalline Solids*, **2018**, *493*, 108-118. [Crossref], [Google Scholar], [Publisher]

[26]. V. Dhivya, G. Rajkumar, S. Mahalaxmi, K. Rajkumar, B. Saravana Karthikeyan, S. Kavitha, R. Karpagam, K. Sakthipandi, G.K. Sathishkumar, Impact of silver on fluorophosphate glasses to improve in vitro bioactivity and antibacterial efficacy, *Ceramics International*, **2022**, *48*, 25346-25354. [Crossref], [Google Scholar], [Publisher]

[27]. W.H. Zachariasen, The atomic arrangement in glass, *Journal of the American Chemical Society*, **1932**, *54*, 3841-3851. [Crossref], [Google Scholar], [Publisher]

[28]. M. Vallet-Regí, A.M. Romero, C.V. Ragel, R.Z. LeGeros, XRD, SEM-EDS, and FTIR studies of in vitro growth of an apatite-like layer on sol-gel glasses, *Journal of Biomedical Materials Research*, **1999**, *44*, 416-421. [Crossref], [Google Scholar], [Publisher]

[29]. P.N. Gunawidjaja, R. Mathew, A.Y.H. Lo, I. Izquierdo-Barba, A. García, D. Arcos, M. Vallet-

Regí, M. Edén, Local structures of mesoporous bioactive glasses and their surface alterations in vitro: Inferences from solid-state nuclear magnetic resonance, *Philosophical Transactions of the Royal Society A*, **2012**, *370*, 1376-1399. [Crossref], [Google Scholar], [Publisher]

[30]. A.M. Beltrán, B. Begines, A. Alcudia, J.A. Rodríguez-Ortiz, Y. Torres, Biofunctional and tribomechanical behavior of porous titanium substrates coated with a bioactive glass bilayer (45S5–1393), *ACS Applied Materials & Interfaces*, **2020**, *12*, 30170-30180 [Crossref], [Google Scholar], [Publisher]

[31]. R. Mathew, P.N. Gunawidjaja, I. Izquierdo-Barba, K. Jansson, A. García, D. Arcos, M. Vallet-Regí, M. Edén, Solid-state ^{31}P and ^{1}H NMR investigations of amorphous and crystalline calcium phosphates grown biomimetically from a mesoporous bioactive glass, *The Journal of Physical Chemistry C*, **2011**, *115*, 20572-20582. [Crossref], [Google Scholar], [Publisher]

[32]. C. Turdean-Ionescu, B. Stevensson, I. Izquierdo-Barba, A. García, D. Arcos, M. Vallet-Regí, M. Edén, Surface reactions of mesoporous bioactive glasses monitored by solid-state NMR: Concentration effects in simulated body fluid, *The Journal of Physical Chemistry C*, **2016**, *120*, 4961-4974. [Crossref], [Google Scholar], [Publisher]

[33]. A. Martínez, I. Izquierdo-Barba, M. Vallet-Regí, Bioactivity of a $CaO–SiO_2$ binary glasses system, *Chemistry of Materials*, **2000**, *12*, 3080-3088. [Crossref], [Google Scholar], [Publisher]

[34]. T.A. Tuan, E.V. Guseva, N.A. Tien, H.T. Anh, B.X. Vuong, L.H. Phuc, N.Q. Hien, B.T. Hoa, N.V. Long, Hydrothermal assisted conventional sol-gel method for synthesis of bioactive glass 70S30, *Matter Interphases*, **2021**, *23*, 585-593. [Crossref], [Google Scholar], [Publisher]

[35]. B.T. Hoa, H.T.T. Hoa, N.A. Tien, N.H.D. Khang, E.V. Guseva, T.A. Tuan, B.X. Vuong, Green synthesis of bioactive glass $70SiO_2$-30CaO by hydrothermal method, *Materials Letters*, **2020**, *274*, 128032. [Crossref], [Google Scholar], [Publisher]

[36]. C. Pontremoli, I. Izquierdo-Barba, G. Montalbano, M. Vallet-Regí, C. Vitale-Brovarone, S. Fiorilli, Strontium-releasing mesoporous bioactive glasses with anti-adhesive zwitterionic surface as advanced biomaterials for bone tissue regeneration *Journal of Colloid and Interface Science*, **2020**, *563*, 92-103 [Crossref], [Google Scholar], [Publisher]

[37]. S. Akhtach, Z. Tabia , K. El. Mabrouk, M. Bricha, R. Belkhou, A comprehensive study on copper incorporated bio-glass matrix for its potential antimicrobial applications, *Ceramics International*, **2021**, *47*, 424-433. [Crossref], [Google Scholar], [Publisher]

[38]. M.J. Da Silva, W. Alves, C.F.D.O. Graeff, P.H.P. D'Alpino, Modified synthesis and physicochemical characterization of a bioglass-based composite for guided bone regeneration, *The Scientific World Journal*, **2021**, *2021*, ID 4295433. [Crossref], [Google Scholar], [Publisher]

[39]. A. Balamurugan, G. Sockalingum, J. Michel, J. Fauré, V. Banchet, L. Wortham, S. Bouthors, D. Laurent-Maquin, G. Balossier, Synthesis and characterisation of sol gel derived bioactive glass for biomedical applications, *Materials Letters*, **2006**, *60*, 3752-3757. [Crossref], [Google Scholar], [Publisher]

[40]. X. Kesse, C. Nedelec J.-M. Nedelec, Deeper insights into a bioactive glass nanoparticle synthesis protocol to control its morphology, dispersibility, and composition, *ACS Omega*, **2019**, *4*, 5768–5775. [Crossref], [Google Scholar], [Publisher]

[41]. S.L. Greasley, S.J. Page, S. Sirovica, S. Chen, R.A. Martin, A. Riveiro, J.V. Hanna, A.E. Porter, J.R. Jones, Controlling particle size in the Stöber process and incorporation of calcium, *Journal of Colloid and Interface Science*, **2016**, *469*, 213-223. [Crossref], [Google Scholar], [Publisher]

[42]. K. Zheng, M. Lu, Y. Liu, Q. Chen, N. Taccardi, N. Hüser, A.R. Boccaccini, Monodispersed lysozyme-functionalized bioactive glass nanoparticles with antibacterial and anticancer activities, *Biomedical Materials*, **2016**, *11*,

035012. [Crossref], [Google Scholar], [Publisher]

[43]. C.J. Shih, H.T. Chen, L.F. Huang, P.S. Lu, H.F. Chang, I.L. Chang, Synthesis and in vitro bioactivity of mesoporous bioactive glass scaffolds, *Materials Science and Engineering: C*, **2010**, *30*, 657-663 [Crossref], [Google Scholar], [Publisher]

[44]. a) G. Kaur, G. Pickrell, N. Sriranganathan, V. Kumar, D. Homa, Review and the state of the art: Sol–gel and melt quenched bioactive glasses for tissue engineering, *Journal of Biomedical Materials Research Part B: Applied Biomaterials*, **2016**, *104*, 1248-1275. [Crossref], [Google Scholar], [Publisher] b) A. Heidaripour, F. Salmani, T. Barati, Synthesis of coral-like ZnO nanostructures with high and wide absorption range, *Asian Journal of Green Chemistry*, **2023**, *7*, 140-148. [Crossref], [Google Scholar], [Publisher]

[45]. S. Chitra, P. Bargavi, S. Balakumar, Effect of microwave and probe sonication processes on sol-gel-derived bioactive glass and its structural and biocompatible investigations, *Journal of Biomedical Materials Research Part B: Applied Biomaterials*, **2020**, *108*, 143-155. [Crossref], [Google Scholar], [Publisher]

[46]. F. Kermani, S. Kargozar, Z. Tayarani-Najaran, A. Yousefi, S.M. Beidokhti, M.H. Moayed, Synthesis of nano HA/βTCP mesoporous particles using a simple modification in granulation method, *Materials Science and Engineering: C*, **2019**, *96*, 859-871. [Crossref], [Google Scholar], [Publisher]

[47]. W.H. Lu, K.D. Li, C.H. Lu, L.G. Teoh, W.H. Wu, Y.C. Shen, Synthesis and characterization of mesoporous $SiO_2CaOP_2O_5$ bioactive glass by solgel process, *Materials Transactions*, **2013**, *54*, 791-795. [Crossref], [Google Scholar], [Publisher]

[48]. H. El Boujaady, M. Mourabet, A. EL Rhilassi, M. Bennani-Ziatni, R. El Hamri, A. Taitai, Adsorption of a textile dye on synthesized calcium deficient hydroxyapatite (CDHAp): Kinetic and thermodynamic studies, *Journal of Materials and Environmental Science*, **2016**, *7*, 4049-4063. [Crossref], [Google Scholar], [Publisher]

[49]. O. Eje, C. Ogbonna, C. Onoyima, F. Nduka, Huntington disease: Mechanism of pathogenesis and recent developments in its therapeutic strategies-A short review, *Journal of Chemical Reviews*, **2023**, *5*, 129-142. [Crossref], [Google Scholar], [Publisher]

[50]. U. Tariq, Z. Haider, K. Chaudhary, R. Hussain, J. Ali, Calcium to phosphate ratio measurements in calcium phosphates using LIBS, *Journal of Physics: Conference Series*, **2018**, *1027*, 012015. [Crossref], [Google Scholar], [Publisher]

[51]. S. Maghsoudi, S.A. Hosseini, S. Ravandi, A Review on phospholipid and liposome carriers: Synthetic methods and their applications in drug delivery, *Journal of Chemical Reviews*, **2022**, *4*, 346-363. [Crossref], [Google Scholar], [Publisher]